Joffre, E., Zamaro, M., Silva, N., Marcos, A., Simplicio, P. V. M., & Richardson, B. (2017). *Results of new guidance and control strategies for landing on small bodies*. Paper presented at International ESA conference on guidance, navigation & control systems, Salzburg, Austria.

Peer reviewed version

GNC 2017 : 10th International ESA Conference on Guidance, Navigation & Control Systems
29 May - 2 June 2017, Salzburg, Austria
European Space Agency

RESULTS OF NEW GUIDANCE AND CONTROL STRATEGIES FOR LANDING ON SMALL BODIES

Eric Joffre[1], Mattia Zamaro[1], Nuno Silva[1], Andrés Marcos[2], Pedro Simplício[2], Barbara Richardson[3]

[1] *Airbus Defence and Space, Gunnels Wood Road, Stevenage SG1 2AS, UK , +44 (0) 1438 773561, eric.joffre@airbus.com*
[2] *University of Bristol, Queen's Building, University Walk, Bristol BS8 1TR, UK , +44 (0) 117 954 5607, andres.marcos@bristol.ac.uk*
[3] UK Space Agency, Polaris House, North Star Avenue, Swindon SN2 1SZ , +44 (0) 1793 41 8061, barbara.richardson@ukspaceagency.bis.gsi.gov.uk

ABSTRACT

While common Descent and Landing strategies involve extended periods of forced motion, significant fuel savings could be achieved by exploiting the natural dynamics in the vicinity of the target. However, small bodies are characterised by perturbed and poorly known dynamics environments, calling for autonomous guidance, navigation and robust control. Airbus and the University of Bristol have been contracted by the UKSA to investigate the optimisation of landing trajectories, including novel approaches from dynamical systems theory, and robust control techniques. This paper presents these techniques with an application to the strategic case of a mission to Phobos.

1 INTRODUCTION

Space sample return missions have a record of revolutionising planetary science. In 2012, new chemical analyses carried out by the University of Chicago on the lunar material collected by Apollo 14 fifty years earlier brought new elements to the disputed question of the origin of the Moon, casting a new doubt on the most widely accepted *Giant Impact* theory [7]. Among the future candidates for exploration missions are the low-gravity and irregularly-shaped Martian moons. In particular, Phobos as a destination is receiving significant attention from the international community both for the wide scientific interest to finally solve the unknowns surrounding the nature of its formation, and because such a precursor mission could represent the technology drive to test some of the key components for a future international Mars Sample Return mission. The results of the analysis on Earth of a sample from Phobos will also characterise the exploitable in-situ resources, possibly enabling to use the moon as a waypoint for the future human exploration of the Martian System.
Close proximity operations including descent and landing are some of the most critical phases for sample return missions, typically characterised by very challenging propellant consumption requirements. While common descent strategies involve an extended period of forced motion, either by translating to the surface from a close hovering station-keeping point or by starting the descent from a distant quasi-satellite orbit, significant fuel savings could be achieved by further exploiting the natural

dynamics in the vicinity of the target. However, a common characteristic of the gravitational environments around asteroids and small bodies like Phobos is that they are both highly perturbed and essentially poorly known, calling for the development of reliable autonomous guidance, navigation and robust control strategies.
As prime contractor for the European Space Agency's *Phobos Sample Return* Phase A study, Airbus has been working towards the definition and preliminary design of a Phobos Sample Return spacecraft and mission. In parallel to this ESA system study, Airbus and the University of Bristol have been awarded a grant by the UK Space Agency to investigate innovative strategies for the design and optimisation of the landing trajectories, as well as robust nonlinear guidance and control techniques.

Figure 1: Colour composite of Phobos taken by ExoMars TGO in November 2016 (left) [Credits: ESA/Roscosmos/CaSSIS] and artist's view of a Phobos Lander (right)

2 PHOBOS SAMPLE RETURN MISSION AND ASSOCIATED CONSTRAINTS

The Phobos Sample Return Phase A study is the continuation of the Phootprint pre-phase A, conducted by Airbus in 2014, with the renewed high-level objective to bring back 100 g of the moon surface regolith back to Earth for analysis. Reference mission scenarios and associated spacecraft designs have been baselined for the mission, including a joint ESA-Roscosmos scenario, with a Proton-M[1] launch from Baikonour in 2024 (baseline) or 2026 (backup), followed by an interplanetary transfer of about 11 months, and an ESA standalone scenario, with an Ariane 5 ECA[1] launch from Kourou in 2024/2025 (baseline) or 2026 (backup), followed by an interplanetary transfer of about 2 years. After a Mars Orbit Insertion (MOI) bringing the spacecraft into a highly elliptical orbit, a sequence of manoeuvres puts the spacecraft on a Quasi-Satellite Orbit (QSO) around *Deimos* for a first science phase to characterise Mars's smaller moon, orbiting the planet at about 20,000 km. Then, manoeuvres are performed to reach a *Phobos* QSO, for a new characterisation phase aimed at identifying the preferred landing sites. After a minimum of 3 fly-by trajectories for high resolution measurements of potential landing sites at low altitudes (typically 5 km), and a first rehearsal to ensure equipments are operating nominally, the descent is initiated via a hovering point about 10 km above the surface of Phobos, for communication and navigation purposes. On Phobos's surface, images of the site are communicated to Earth for the selection of the samples, then collected by means of a robotic arm. Following Phobos ascent and return transfer, the Earth Re-entry Capsule (ERC) containing the samples is set to land in either Kazakhstan or Australia.

[1]subject to launchers continued availability, the Angara-5 and Ariane 64 Launch Vehicles being planned to progressively replace Proton and Ariane 5 ECA respectively, at dates that are not presently known.

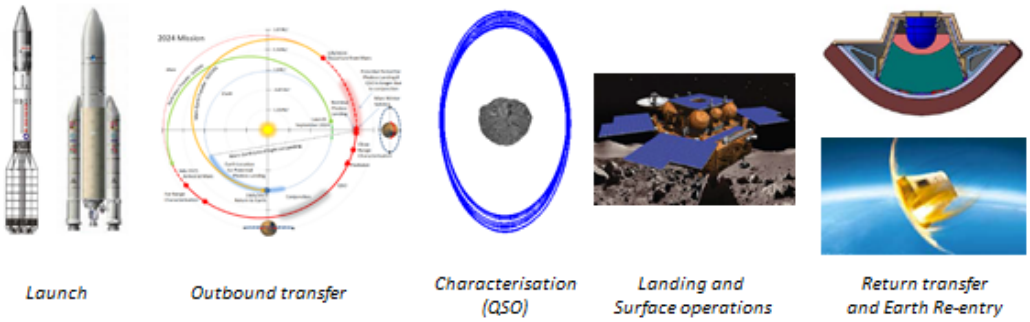

Figure 2: Phobos Sample Return main mission phases

The work presented in this paper investigates alternative landing strategies that take further advantage of the natural dynamics in the vicinity of the small body. Specific requirements applicable to the landing include the following:

- 20% accessibility of Phobos surface (goal is 50%), including latitudes up to 60 deg
- landing accuracy on Phobos better than 50 m at a 95 % confidence level
- landing velocities at Phobos: vertical < 1.5 m/s, horizontal < 1 m/s
- final free-fall (without using thrusters) of 20 m, to avoid surface contamination

3 MISSION ANALYSIS AND REFERENCE LANDING TRAJECTORY DESIGN

The objective of this section is to describe the dynamics environment applicable for the study, the models used for the simulations, and the derivation of reference open-loop landing trajectories.

3.1 Dynamics in the vicinity of Phobos and reference frames

Mars largest moon Phobos is a small body with dimensions 13.1 km $\times$ 11.1 km $\times$ 9.3 km (mean ellipsoid), orbiting the Red Planet at a mean altitude of less than 6,000 km and a period of about 7 hours and 40 minutes[2]. The next table provides some physical constants and orbital parameters[3] used in the study, both for Mars (orbit around the Sun) and Phobos [3] (orbit around Mars).

Table 1: Main physical properties and orbital parameters used for Mars and Phobos

Body	Gravity μ_g $(m^3 s^{-2})$	Mass (kg)	Semi-major axis (km)	Eccentricity	Inclination (deg)
Mars	4.2828×10^{13}	6.4185×10^{23}	227.9478×10^{6}	0.0934	0.0323
Phobos	711200	1.0659×10^{16}	9379.2557	0.0156	0.0186

Given the low value for Phobos' orbit eccentricity, the first level of approximation for the dynamics of a spacecraft in the Mars-Phobos system is given by the *Circular Restricted Three Body Problem*

[2] shorter than the Mars rotation period: an observer on Mars would see Phobos rise in the West and set in the East.
[3] Source: NASA JPL ephemeris at epoch 25 July 2012 00.00 UTC

(CRTBP) [12]: even though this model is simplified, it gives some insight into the main characteristics of the dynamics. In particular, given the reduced mass ratio of $m_{\text{Phobos}}/(m_{\text{Mars}} + m_{\text{Phobos}}) = 1.65 \times 10^{-8}$, and the dimensions of Phobos, the L1 and L2 collinear Libration Points of the Mars-Phobos system lie only a few kilometers (about 3.5 km) above the surface of the moon. An important consequence of this property is that there is no possibility for a Keplerian orbit around Phobos, and the third-body perturbation of Mars gravity cannot be neglected for the design and simulation of descent and landing trajectories[4]. The next figure shows the location of the L1 and L2 Lagrangian points assuming a CRTBP model, together with the (in-plane) *zero-velocity curves* associated with their corresponding levels of Jacobi Integral [12].
The dominant perturbations to this model are the *ellipticity* of Phobos' orbit around Mars, and the *non-spherical gravitational field* of Phobos [14] : owing to its high inhomogeneity and very irregular shape, the gravity field of the moon cannot be described properly by a spherical (Keplerian) potential. Using spherical coordinates r for the radius, θ for the co-latitude, and ϕ for the longitude, and a reference radius R, the gravity potential is described by a spherical harmonics double expansion:

$$U_g(r,\theta,\phi) = \frac{\mu_{g_{\text{Phobos}}}}{R} \sum_{n=0}^{\infty} \left(\frac{R}{r}\right)^{n+1} \sum_{m=0}^{n} C_n^m(\phi) P_n^m(\cos(\theta)) \tag{1}$$

$$\text{where:} \quad \begin{cases} C_n^m(\phi) &= C_{n,m}\cos(m\phi) + S_{n,m}\sin(m\phi) \\ P_n^m(x) &= (1-x^2)^{m/2}\dfrac{d^m}{dx^m}P_n(x) \\ P_n(x) &= \dfrac{1}{2^n n!}\dfrac{d^n}{dx^n}(x^2-1)^n \end{cases} \tag{2}$$

The next figure illustrates the location of the CRTBP L1 and L2 Lagrangian points, and provides the Gravity Harmonics coefficients $C_{n,m}$ and $S_{n,m}$ for a reference radius of $R = 11$ km [1].
Mars non-spherical gravitational perturbation, and in particular its first zonal coefficient J_2 due to the planet's oblateness, also has a non-negligible contribution, but it remains one order of magnitude below the aforementioned perturbations for the application considered.
The previous figure 3.1 also illustrates the reference frames used in the study:

- The Hill frame has its origin at the moon's barycentre and rotates with a fixed attitude with respect to its orbit around Mars: the vertical z-axis is perpendicular to the orbital plane, and the radial x-axis is pointing outwards from the Mars-Phobos barycentre. This is the usual frame considered for the description of the motion in a three-body problem.

- The Body-Centred Body-Fixed frame (BCBF) also has its origin at the moon's barycentre but its attitude is fixed with respect to the body's geometry: the vertical z-axis is aligned along the body's spin axis, and the x-axis is pointing towards the intersection of a body's reference Prime Meridian and the equatorial plane.

[4]This property, very specific to the Mars-Phobos system, will generally not be observed in the vicinity of another small body, and in particular for an asteroid. Not only thought to be strategic for application in a future Phobos Sample Return mission, the Phobos study case has been selected as a challenging dynamical system capturing all the nonlinearity of a three body problem, to test the robustness and performance of the landing guidance and control.

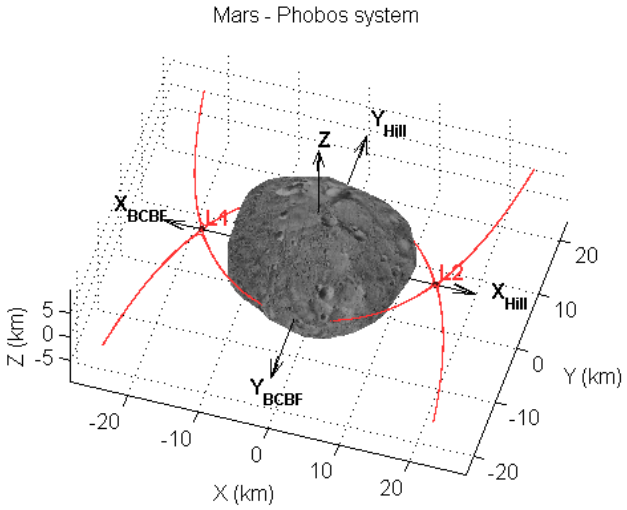

(n,m)	$C_{n,m}$	$S_{n,m}$
(2,0)	-0.04698	0
(2,1)	0.00136	0.00138
(2,2)	0.02276	-0.000202
(3,0)	0.00293	0
(3,1)	-0.00309	0.00181
(3,2)	-0.00847	-0.000655
(3,3)	0.00224	-0.01392
(4,0)	0.00762	0
(4,1)	0.00347	-0.000776
(4,2)	-0.00288	-0.00112
(4,3)	-0.0028	0.00337
(4,4)	-0.0012	-0.000622

Figure 3: Phobos reference frames, CRTBP Lagrangian Points L1, L2 and associated in-plane zero-velocity curves (left), gravity harmonics coefficients [1] (right)

As a long-term effect of Mars' gravity gradient (tidal force), Phobos has the interesting property that its revolution around Mars and rotation around its spin axis are synchronous, and almost non-tilted: Phobos is said to be *tidally locked*, like our Moon, always showing the same face to the planet. With this approximation, Hill and BCBF frames z-axes are coincident, while their x-axes differ only by the definition of the Prime Meridian. In reality, an additional oscillation between a minimum of 0.30 deg and a maximum of 1.90 deg is observed. However the dynamics of this motion, seen from Phobos as a Mars' libration in latitude is much slower (period of 2.26 terrestrial years) than the time-scale of a mission segment around Phobos [13].

3.2 Dynamics models: Mission Analysis and Guidance (MAG) and Dynamics, Kinematics and Environment (DKE)

The BCBF frame is the most natural coordinate system to be used for a landing problem, and will serve as the reference frame for the expression of the equations of motion, as well as all subsequent trajectory representations in the next sections. As the main challenge to be addressed in the context of the study is the derivation of robust closed-loop landing strategies in perturbed and poorly known environments, two different models for the descent and landing have been implemented:

- A first model is considered to represent the dynamics environment that would be used on the ground for the mission analysis, the definition and design of sets of reference landing trajectories. Assumed to be representative enough of the dynamics in flight, this is also the model to be used by the on-board guidance function. Therefore, this model will be referred to as the *Mission Analysis and Guidance* (MAG) model.

- As the dynamics in orbit will differ from the dynamics predicted on the ground, and in order to be able to assess the robustness of closed-loop landing guidance and control, a second model is needed to simulate the *actual* dynamics experienced by the spacecraft. This model will be referred to as the *Dynamics, Kinematics and Environment* (DKE). This model is a statistical model with some parameters drawn from predefined probability distributions: each DKE simulation is a single realisation of the statistical model. It also includes second order perturbations such as Mars' J_2 and Mars' libration apparent motion from Phobos's BCBF frame, not included in the MAG model.

Based on the previous description of the various contributors to the orbital dynamics in the vicinity of Phobos, the next table summarises the assumptions considered for each of these models:

Table 2: Difference of assumptions for the MAG and DKE dynamics models

	Dynamics model	
Contributors	MAG	DKE
Mars gravity model	Keplerian (Spherical potential)	Kepler + J_2 (GHs = first zonal coefficient)
BCBF wrt Hill	Fixed and non-tilted (equatorial)	Librating
Phobos gravity model	Full GHs $(m = 4, n = 4)$ Deterministic	Full GHs $(m = 4, n = 4)$ Probabilistic
Probabilistic parameters	None	GHs coefficients $C_{n,m}$ and $S_{n,m}$ $\mathcal{N}(\mu_{\text{MAG}}, \sigma = 100\%\|\mu_{\text{MAG}}\|)$

The equations of motion are fairly complex, to account for all the effects described above, but they can be written in a generic state-space form, with the state vector $\underline{X}$ (BCBF position and velocity), vector field f (MAG or DKE), command matrix B and propulsive acceleration $\underline{U}$, as:

$$\dot{\underline{X}} = f(\underline{X}, t) + B \cdot \underline{U} \tag{3}$$

Due to Phobos' orbit ellipticity, the system is non autonomous and it must be augmented with an equation for Phobos true anomaly ν on its orbit around Mars. This standalone equation can be written as follows, e being Phobos orbit eccentricity and n its mean motion:

$$\dot{\nu} = n\frac{(1 + e\cos(\nu))^2}{(1 - e^2)^{3/2}} \tag{4}$$

3.3 Initial guess for landing trajectories using Libration Point Orbits and invariant manifolds

As described in the previous paragraph, it is impossible to design an orbit around Phobos that is not strongly perturbed by the gravity of Mars. Therefore, instead of using distant Quasi-Satellite Orbits (QSOs) for the selection of the landing site, followed by a sequence of costly forced manoeuvres for the descent and landing, the solution investigated in this study consists in using Libration Point Orbits (LPOs) as natural close observation platforms, and their invariant manifolds, initiated by a small magnitude ΔV on the LPO, as an *initial guess* for a landing trajectory. In order to simulate such trajectories, the first step is to derive the conditions for suitable LPOs. The derivation of Periodic Orbits [5, 6] (POs) and Quasi-Periodic Orbits [8, 10] (QPOs) in the CRTBP has been studied extensively in the past. The figure 4 below illustrates families of Lyapunov planar, vertical and Halo periodic

orbits around the L1 and L2 Lagrangian Points of the Mars-Phobos system. However, such orbits are unstable and, as the dynamics is strongly perturbed, trying to remain on an LPO computed in the CRTBP would come at a significant station-keeping cost. The procedure used [14] is to *identify* LPOs in the Mars-Phobos-spacecraft CRTBP and then numerically continue a parameter that incrementally increases the effect of perturbations: the gravity harmonics and then the eccentricity. Eventually, families of POs, Quasi-halo and Lissajous QPOs are derived in the full MAG dynamics model. The invariant manifolds associated with all these orbits are then computed and those intersecting with Phobos are selected, as illustrated by the figure below.
If the landing site is not imposed, several trajectories are generally suitable candidates, and can be filtered according to an additional criterion. On the example considered, for each reachable landing site, the manifold with the highest incidence at touch-down (the most vertical) is selected. Finally the landing site is chosen as the one with the lowest touch-down velocity.

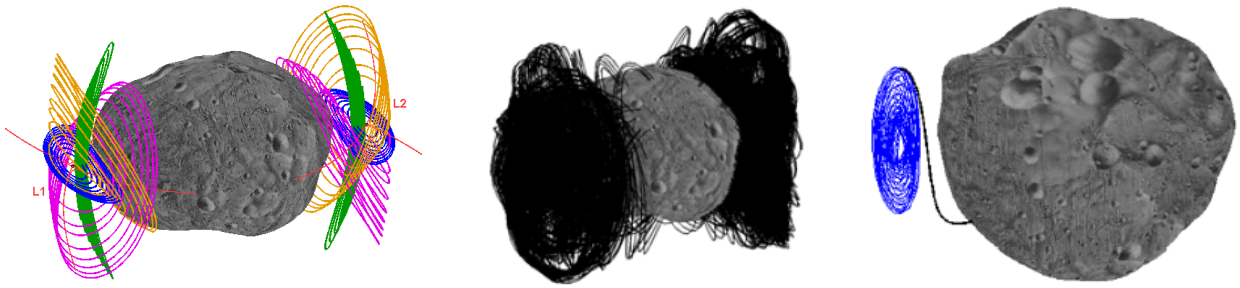

Figure 4: L1 and L2 POs (left), manifolds interesecting Phobos (middle) and selected manifold (right)

3.4 Soft landing manifold trajectory optimisation

The next step consists in implementing thrust to command the spacecraft to the landing site $\underline{r}_f$ with zero velocity $\underline{v}_f = 0$ at touch-down, as it would generally not be the case for a ballistic manifold.[5] The Open-Loop Guidance (OLG) profile is searched as a fixed order polynomial expression between $t_b > t_0$ and $t_f > t_b$, with time normalised by Phobos orbital period T.

$$\underline{U}(t > t_b) = \sum_{k=0}^{n} \underline{U}_k \left(\frac{t - t_b}{T} \right)^k \tag{5}$$

Such a fixed structure parametrisation of the OLG profile will lead to a suboptimal solution, but it has two important advantages: first, it is easy to implement in an on-board software, and besides it allows using parametric Nonlinear Programming (NLP) algorithms with a reduced set of parameters, for a faster optimisation process. The objective is to minimise the propulsive ΔV, while keeping an admissible level of error on the final state:

$$\min_{t_b, t_f, \{\underline{U}_k\}_{k \in [\![0,n]\!]}} J(t_b, t_f, \{\underline{U}_k\}_{k \in [\![0,n]\!]}) = \int_{t_0}^{t_f} \|\underline{U}(t)\| dt + \Psi \cdot \left[\underline{X}(t_f) - \underline{X}_f \right] \tag{6}$$

[5] In the context of this work, no final free fall requirement has been considered for the derivation of the Open-Loop Guidance and subsequent closed-loop tests. This is without loss of generality as it would only modify the numerical values for the target position $\underline{r}_f$ and velocity $\underline{v}_f$, the free fall problem being addressed separately.

The parameter Ψ is a penalisation matrix on the final state error[6], and can be tuned so that the desired landing accuracy is achieved. The following figure illustrates a solution trajectory reached, using the ballistic manifold described in the previous section as the initial guess. Arrows represent the direction and relative magnitude of the optimal OLG propulsive acceleration.

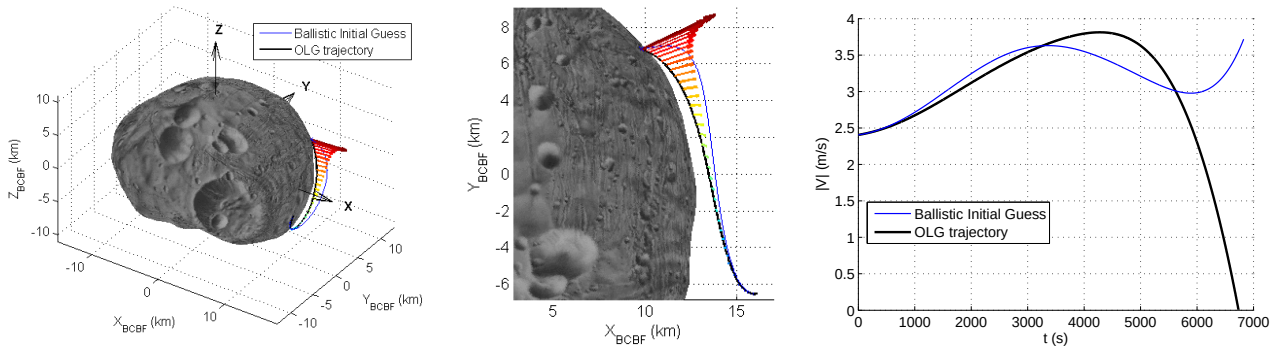

Figure 5: Optimised manifold landing trajectory, and velocity profile

As is apparent on the previous plot, the thrusters are activated as soon as the spacecraft leaves the LPO. Local optima were reached by the optimiser with different values of $t_b > t_0$, when initialised with initial guesses far from t_0. However, as a general rule, and despite the fact that the thrust duration is less, the required propulsive acceleration is significantly increased, and its time integral, which corresponds to the propulsive ΔV, is increased as well. The optimised open-loop soft landing has a duration of less than 2 hours and requires a propulsive ΔV of about 7 m/s.

3.5 Forced translation descent trajectory optimisation

In order to compare the manifold-based landing to a more classical approach, a second open-loop reference trajectory is computed as a forced translation from a hovering Station-Keeping (SK) point 10 km above the surface towards the same landing site, along the local normal to the surface. This case is easier since a parametric analytical expression of the reference *kinematics* can be given so as to meet the soft landing requirement. A simple admissible solution is given by a trapezoidal profile, described by only four parameters (Δt_1, Δt_2, v_d, t_f) to fully define the descent kinematics: by integration of this continuous piecewise function, one naturally derives the following analytical expressions, with initial, final and continuity constraints used to obtain the integration constants.

Table 3: Kinematics equations for the forced translation

Time interval	Position	Velocity	Total Acceleration
$t \in [t_0, \Delta t_1]$	$\underline{r}(t) = \underline{r}_0 + \frac{\underline{v}_d t^2}{2\Delta t_1}$	$\underline{v}(t) = \frac{\underline{v}_d t}{\Delta t_1}$	$\underline{a}(t) = \frac{\underline{v}_d}{\Delta t_1}$
$t \in [\Delta t_1, t_f - \Delta t_2]$	$\underline{r}(t) = \underline{r}_0 + \underline{v}_d \left(t - \frac{\Delta t_1}{2} \right)$	$\underline{v}(t) = \underline{v}_d$	$\underline{a}(t) = 0$
$t \in [t_f - \Delta t_2, t_f]$	$\underline{r}(t) = \underline{r}_f - \frac{\underline{v}_d (t_f - t)^2}{2\Delta t_2}$	$\underline{v}(t) = \frac{\underline{v}_d (t_f - t)}{\Delta t_2}$	$\underline{a}(t) = -\frac{\underline{v}_d}{\Delta t_2}$

[6]The notation $\left[\underline{X}(t_f) - \underline{X}_f\right]$ represents the vector of the *norms* of each component of the error vector.

An additional constraint is imposed by the continuity of the position of the spacecraft at $t = t_f - \Delta t_2$, reducing the number of free parameters down to three. The propulsive acceleration required is obtained as the difference between the total acceleration and the apparent gravitational acceleration given by the MAG vector field velocity components:

$$\underline{U}(t) = \underline{a}(t) - f_v(\underline{X}, t) \tag{7}$$

This time the soft landing requirement is ensured by design, and the ΔV minimisation problem to solve can be written again as a parametric minimisation problem, with a single inequality:

$$\min_{\Delta t_1, \Delta t_2, t_f \geq \Delta t_1 + \Delta t_2} J(\Delta t_1, \Delta t_2, t_f) = \int_{t_0}^{t_f} \|\underline{U}(t)\| dt \tag{8}$$

The following figures illustrate the solution trajectory reached, the arrows representing the direction and relative magnitude of the optimal OLG propulsive acceleration. The solution is such that the trapezoidal profile degenerates into a triangular profile with $\Delta t_1 + \Delta t_2 = t_f$ (active constraint).

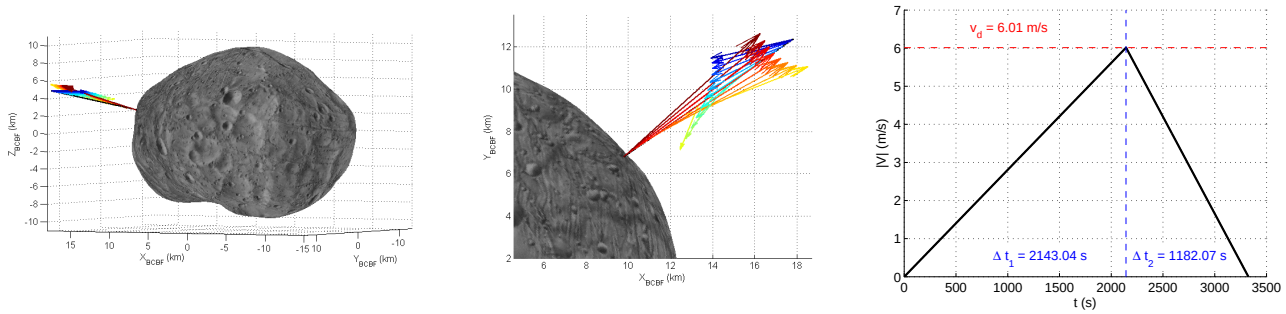

Figure 6: Optimised forced translation landing trajectory and velocity profile

The illustrated forced translation landing has a duration of less than 1 hour and requires a propulsive ΔV of about 16.5 m/s, which is significantly higher than the previous manifold-based trajectory. In addition, the hovering station-keeping point needs to be maintained prior to landing, at an average[7] cost of about 50 m/s per Phobos orbital period or 6.9 m/s per hour.

4 CLOSED-LOOP GUIDANCE IMPLEMENTATION

In the previous section, open-loop command profiles (referred to as Open-Loop Guidance OLG) have been derived in the dynamics environment described by the MAG model. When injected in a realisation of the DKE model to simulate the *actual* dynamics experienced by the spacecraft, the OLG command profile generally steers the spacecraft on a trajectory that rapidly diverges from the nominal trajectory. The next figure illustrates the observed behaviour when simulating the manifold-based OLG in a Monte-Carlo campaign of 200 DKE runs with dispersed Phobos Gravity Harmonics. As evidenced by the left figure, some trajectories actually crash on Phobos while others never reach its surface (single DKE realisation example on the right), demonstrating the importance of the perturbations on the dynamics, and calling for the implementation of robust closed-loop strategies.

[7]The instantaneous SK cost depends on Phobos true anomaly, and the spacecraft's altitude, latitude and longitude.

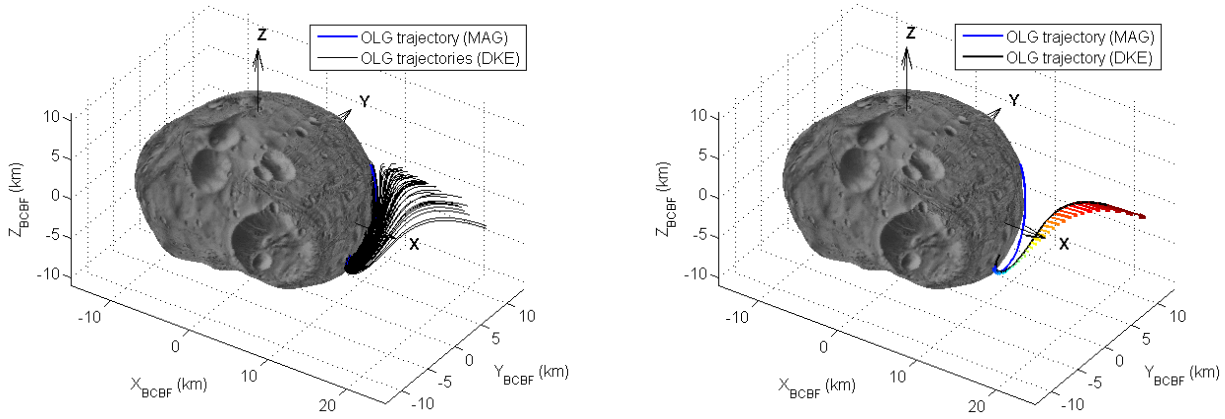

Figure 7: DKE simulations using the manifold landing trajectory OLG command profile

4.1 Guidance problem

The role of the *guidance* function is to compute, from the estimation of the current state of the spacecraft, the command and associated trajectory to follow so as to meet the mission's objectives, while respecting a given set of constraints and generally optimising a performance index. This function can be implemented either on the ground or directly in the on-board software, with a variety of possible intermediate architectures and subsequent impacts on the overall concept of operations. In the context of the present study, the objective is to maximise the autonomy of the spacecraft for the descent and landing phase: given the possibly long communication delays[8] as compared to the phase duration, the spacecraft should be able to complete its mission autonomously as soon as the descent is initiated. Ideally, the guidance optimisation problem solved in real-time should be the same optimisation problem as the one considered for the mission analysis on the ground before the mission for the derivation of reference trajectories, only replacing the initial state by the actual (estimated) state at the current guidance step, as schematically illustrated below.

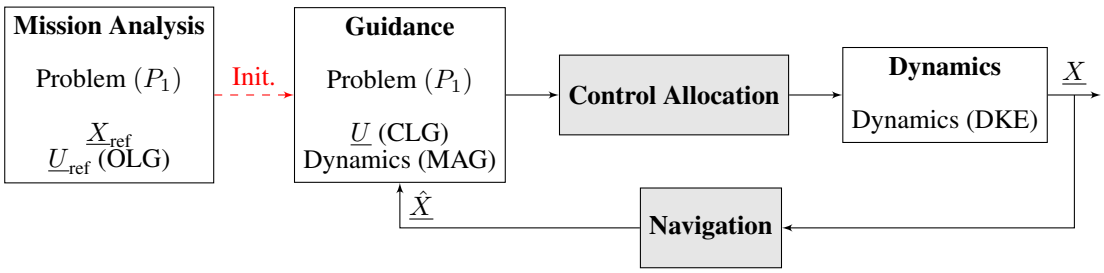

Figure 8: Fully explicit Closed-Loop Guidance (CLG) architecture[9]

[8] Depending on the orbital configuration of the planets, round-trip communication times between the Earth and Mars can take from under 10 minutes up to more than 40 minutes.

[9] The control allocation and navigation functions are very system-dependent and not described in this paper: respectively on the propulsion system and thruster configuration, and on the sensor suite and estimation algorithms, both beyond the scope of the study.

Such an approach is sometimes called *fully explicit* Closed-Loop Guidance (CLG): in this case the pre-computed OLG profile is not used, or only to initialise the optimisation process. Conversely, a *fully implicit* strategy would use directly the OLG with no feedback of the estimated state to recalculate the command, which has been demonstrated to be inapplicable for our problem. In most cases however, the resolution of the full optimisation problem is not compatible with the on-board computational resources and/or time constraints, so that the guidance optimisation problem must be simplified. This simplification can arise from the description of the dynamics, the expression of the constraints, or even the selection of the performance index. A typical example for a space trajectory guidance strategy is to use a *quadratic* performance index to derive so-called *energy optimal* trajectories, instead of a more natural cost functional that would be associated with the *propellant consumption*:

$$J_{\mathcal{L}_1}(\underline{U}) = \int_{t_0}^{t_f} \|\underline{U}(t)\| dt \quad ; \quad J_{\mathcal{L}_2}(\underline{U}) = \int_{t_0}^{t_f} \|\underline{U}\|^2(t) dt \tag{9}$$

- From a mission perspective, $\mathcal{L}_1$ is a more appropriate definition of the actuation cost: it is associated with the propulsive ΔV, and therefore the propellant consumption. Such problems are generally challenging to solve, characterised by non-smooth solutions[10], requiring iterative and computationally demanding methods. Reference OLG were derived using $\mathcal{L}_1$ cost functionals.
- Conversely, quadratic ($\mathcal{L}_2$) optimisation problems are generally easier to solve numerically (smooth solutions) and in case the dynamics is simple, analytical solutions may even be found.

As a consequence, quadratic ($\mathcal{L}_2$) optimisation problems are generally well adapted for on-board closed-loop guidance schemes, while minimum propellant consumption $\mathcal{L}_1$ optimisation problems are considered for the derivation of reference trajectories. However, propellant mass penalties are expected to be incurred from the resolution by the guidance function of a distinct optimisation problem.

4.2 Guidance survey for autonomous planetary landing

Closed-loop guidance for autonomous landing has been the focus of several studies in the past twenty years. Most surveyed techniques, such as those presented in the next table, provide simple analytical laws, derived under highly simplified exogenous conditions, and not always seeking optimality.

Table 4: Classical and optimal autonomous guidance schemes analytical expressions

Classical	Proportional Navigation Guidance (PNG)	$\underline{U} = kV_c\dot{\underline{\Lambda}}$
	Augmented PNG (APNG)	$\underline{U} = kV_c\dot{\underline{\Lambda}} - \frac{k}{2}\underline{g}_{\perp}$
	Biased PNG (BPNG)	$\underline{U} = 4V_c\dot{\underline{\Lambda}} - \underline{g} + \frac{2V_c}{t_{\text{go}}}(\underline{\Lambda} - \underline{\Lambda}_f)$
Optimal	Free Terminal Velocity Guidance (FTVG)	$\underline{U} = \frac{3}{t_{\text{go}}^2}(\underline{r}_f - \underline{r}) - \frac{3}{t_{\text{go}}}\underline{v} - \frac{3}{2}\underline{g}$
	Constrained Terminal Velocity Guidance (CTVG)	$\underline{U} = \frac{6}{t_{\text{go}}^2}(\underline{r}_f - \underline{r}) - \frac{4}{t_{\text{go}}}\underline{v} - \underline{g} - \frac{2}{t_{\text{go}}}\underline{v}_f$
	FTVG ZEM-ZEV formulation	$\underline{U} = \frac{3}{t_{\text{go}}^2}\underline{ZEM}$
	CTVG ZEM-ZEV formulation	$\underline{U} = \frac{6}{t_{\text{go}}^2}\underline{ZEM} - \frac{2}{t_{\text{go}}}\underline{ZEV}$

[10]The fact that the solutions are singular does not mean that they are not achievable: saturated *bang-bang* like optimal control solutions may actually be more representative of the physical operating of a spacecraft propulsion system.

An extensive survey and analysis of closed-loop guidance for autonomous landing has been the object of a dedicated paper [11] and will not be further described here.

4.3 Guidance implementation and preliminary results

Among the above guidance schemes, the Constrained Terminal Velocity Guidance (CTVG) is the most appropriate as it results from an optimal control problem formulation with a fixed final *full* state, including the velocity. Its direct implementation in the closed-loop model including the *DKE* dynamics can be performed by taking at each guidance step t: the apparent gravitational acceleration given by the *MAG* vector field velocity components at the estimated current state $\underline{g} = f_v(\underline{\hat{X}}, t)$, and the remaining time until the end of the reference open-loop trajectory as the time-to-go. Considering perfect navigation and actuation as well as a time-continuous closed-loop guidance correction for a preliminary assessment, the trajectory meets the landing requirements, reaching the target at zero velocity with a good accuracy. However, this direct implementation has the following limitations:

- The absence of path constraints implies that it is not possible to prevent trajectories that would theoretically reach the desired final state with intermediate positions passing below the surface of Phobos, actually leading to a crash.
- As foreseen in the previous paragraph and illustrated in the appendix, the ΔV required to follow the closed-loop trajectory is significantly increased as compared to the OLG reference.

The next figure illustrates such an example, starting from the initial conditions of the manifold-based trajectory, but following a very different path and crashing into Phobos. The theoretical ΔV until the final state is reached is 15.4 m/s, which is more than twice the ΔV of the reference OLG.[11]

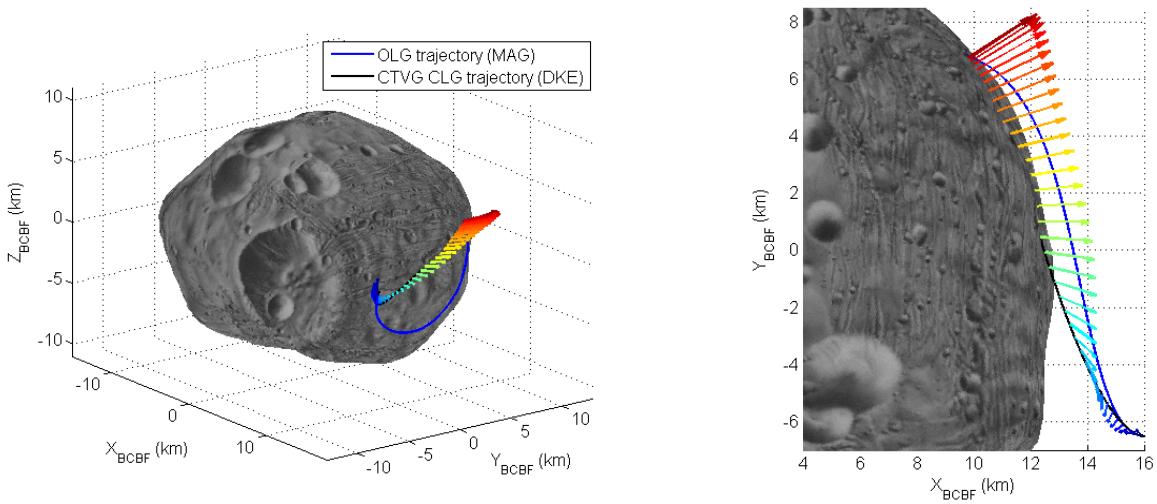

Figure 9: Crashing trajectory with CTVG simplified explicit closed-loop guidance DKE simulation

[11] In the CTVG problem formulation, the final time t_f is fixed, so that a one-dimensional optimisation (line search) of this parameter could be envisaged as part of the guidance command update. However this would lead to consider again an iterative algorithm that was avoided by using an analytical solution of a pre-solved problem.

Both limitations can be addressed by an adaptation of the guidance strategy: instead of targeting at each *guidance step* the *final* reference date and state (landing site with zero-velocity), the time-to-go, or *guidance horizon* (between the current date and the target guidance date), can be reduced to target an intermediary state interpolated on the reference trajectory. A parametric analysis of this strategy has been performed for a range of *guidance steps* t_g and *guidance horizons* $t_h \geq t_g$, still assuming perfect navigation and actuation to focus on the guidance. The accuracy can be measured by the 2-norm of a vector defined by the normalised error on position velocity at the nominal final time t_f.[12]

$$J(\Delta r_f, \Delta v_f) = \left\| \left(\frac{\Delta r_f}{\Delta r_{\text{tol}}}, \frac{\Delta v_f}{\Delta v_{\text{tol}}} \right) \right\|_2 = \sqrt{\left(\frac{\Delta r_f}{\Delta r_{\text{tol}}} \right)^2 + \left(\frac{\Delta v_f}{\Delta v_{\text{tol}}} \right)^2} \tag{10}$$

A few points on the (t_g, t_h) domain are selected for further analysis: statistics (mean and standard deviation) on the propulsive ΔV and landing accuracy are drawn from a Monte-Carlo campaign on the DKE model realisations, and reported in the next tables with $\Delta r_{\text{tol}} = 10$ m and $\Delta v_{\text{tol}} = 10$ cm/s.

Table 5: Parametric performance analysis of the way-point based CTVG - Statistical DKE

$\mu[\Delta V]$ (m/s)		t_g (s)			
		10	100	200	400
t_h (s)	1000	7.34	7.36	7.36	7.66
	2000	8.07	8.16	8.23	8.39
	3000	9.91	10.1	10.3	10.9

$\sigma[\Delta V]$ (m/s)		t_g (s)			
		10	100	200	400
t_h (s)	1000	0.96	0.96	0.95	1.10
	2000	1.05	1.08	1.12	1.08
	3000	1.13	1.17	1.23	1.27

$\mu[J]$ (-)		t_g (s)			
		10	100	200	400
t_h (s)	1000	0.17	0.55	0.68	4.71
	2000	0.15	0.52	0.51	4.63
	3000	0.13	0.45	0.53	5.55

$\sigma[J]$ (-)		t_g (s)			
		10	100	200	400
t_h (s)	1000	0.09	0.26	0.57	2.04
	2000	0.09	0.39	0.41	2.81
	3000	0.09	0.32	0.39	3.71

As could be expected, this analysis shows that the guidance performance is increased for a higher correction frequency (small t_g), which in practice will be limited by the on-board computational time and the delays involved in the overall closed-loop. Regarding the tuning of the guidance horizon, shorter times for $t_h > t_g$ are better for the ΔV, almost asymptotically reaching the reference OLG ΔV, with a lesser impact on the final accuracy, up to a certain limit when the closed-loop actually becomes unstable and the trajectories rapidly diverge from the reference.

4.4 Control implementation

The last phase of the project has investigated augmented guidance strategies specifically aimed at addressing *robustness*. The reformulation of the guidance problem as a tracking-like problem opens the door for a range of control theory applications: by implementing an inner control loop of a linearised model of the dynamics in the vicinity of the reference trajectory, as shown in the next block-diagram, several techniques for the synthesis, tuning and analysis of linear systems become applicable.
The main focus of the University of Bristol within the Project was on the investigation of the application of modern *robust control* techniques for the design and optimisation of Space Descent and

[12] While the state errors at time t_f and the derived J performance index do indeed measure the *guidance* performance as a deviation from the nominal target in state and time, it is not necessarily representative of actual trajectories, as some will have crashed before t_f, and some others may very well reach the surface of Phobos at a later date.

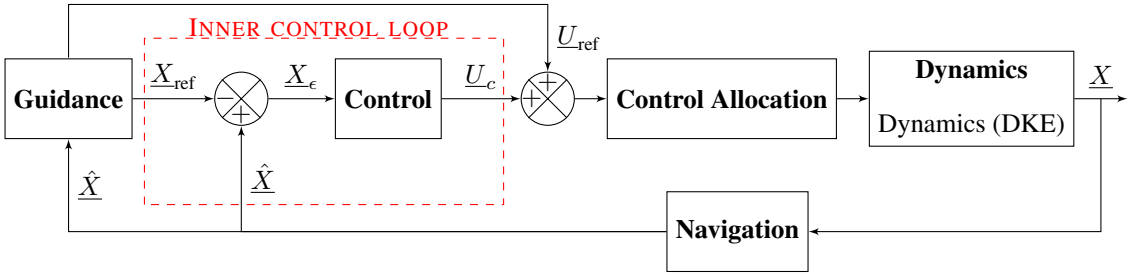

Figure 10: Closed-Loop architecture with control inner loop

Landing trajectories. The Robust Control framework is appealing as it offers the ability to explicitly account for the effects of uncertain gravitational environments, characteristic of small bodies.
The process, illustrated by the next figure, is summarised as follows[13]:

- linearisation of the dynamics model in the vicinity of a reference profile (trajectory and command), yielding a first-order perturbation model,
- capture of the uncertainties (essentially Phobos' gravity harmonics but also actuation errors) in a Linear Fractional Transformation (LFT) representation [2],
- inclusion of time-varying effects through Linear Parameter Variant (LPV) modelling [9],
- synthesis of a robust controller using the structured $\mathcal{H}\infty$ framework [4],
- analytical robustness analysis carried out thanks to μ *analysis* and of *IQC analysis* to assess performance in presence of the gravitational uncertainties, and nonlinear effects respectively.

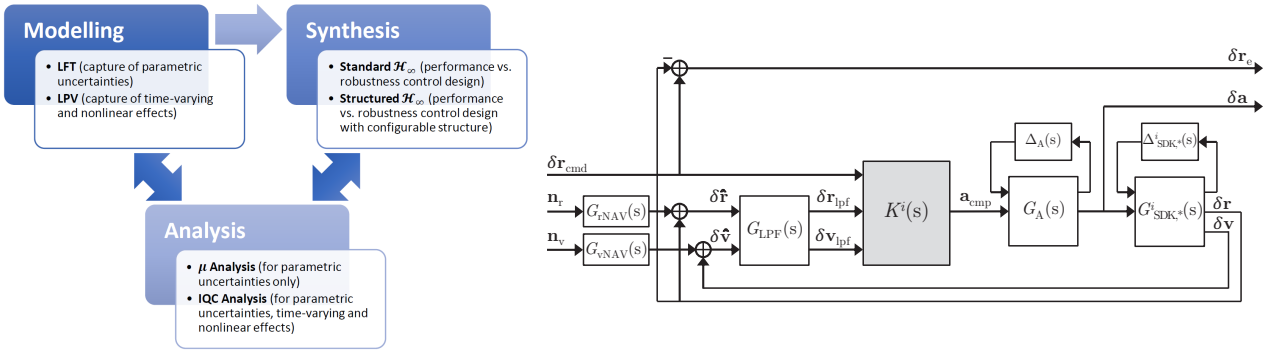

Figure 11: Robust control design workflow and techniques, and model used for the control synthesis

Among the conclusions drawn from the application of this robust control framework, it has been shown that the design and performance are more critically driven by model uncertainties rather than the time-varying effects. Another lesson learnt for the (LFT) modelling of the system is that the

[13] A dedicated paper, currently in preparation, will describe in further detail each step of the above process and its application to landing on Phobos.

performances of the controller are degraded when considering over-conservative uncertainty specifications. Ultimately, considering again perfect navigation, the final time-domain performances of the resulting closed-loop implementation are characterised by a ΔV increase of less than 5% with respect to the nominal open-loop optimal (nominal) profile, while achieving a final accuracy below 1 m in position and 0.01 m/s in velocity.

5 CONCLUSION AND FUTURE WORK

This paper presented the work conducted by Airbus and the University of Bristol on strategies for autonomous landing on small bodies, with a focus on the mission analysis, reference trajectory optimisation, and closed-loop guidance and control assessment. In the challenging framework of a landing on Phobos, Libration Point Orbits have been computed and proposed to be used as natural observation platforms, while their associated manifolds serve as initial guess for optimising a controlled landing trajectory towards a selected landing site. Owing to limited on-board resources, the guidance will have to solve a simpler optimisation problem, at the expense of an increased propellant consumption. This can however be mitigated by making the most of the reference trajectory in a way-point based adaptation of quadratic optimal guidance schemes, while the robustness to the uncertain dynamics environment is efficiently tackled through an inner control loop, designed by means of modern robust control techniques. The overall strategy proved to be compliant with the surface access requirements, and to cope with highly complex and uncertain dynamics environments, also achieving a significant reduction of the propellant consumption when compared to more classical approaches.
Further selection among of the various architectures and options demonstrated to perform properly for an actual Phobos Sample Return mission will be subject to a more detailed set of requirements for the Guidance, Navigation and Control subsystem as the project hopefully progresses to a next phase. In particular, the detailed modelling and performance of the navigation, control allocation and thruster modulation functions as well as other system-level constraints could narrow down the range of possible techniques among the ones investigated in the project. In the meantime, Airbus recently started a new study funded by the UK Space Agency under the CREST (Collaborative Research in Exploration Systems and Technology) programme, to address the trade-off between on-ground and on-board repartition of tasks for the phases prior to the initiation of the final end-game with Phobos, revisiting the *concept of operations* and assessing the opportunity for an increased level of autonomy.

6 ACKNOWLEDGEMENT

This work has been funded by the UK Space Agency (UKSA), under the National Space Technology Programme (NSTP). The authors are thankful to Mick Johnson and Christopher Brownsword, respectively Director and Technical Director of the Centre for Earth Observation and Instrumentation (CEOI), for their support and collaboration in the first months of the project, as well as Barbara Richardson, NSTP Programme Manager and coordinating the project for the UKSA.

REFERENCES

[1] B. F. Chao and D. P. Rubincam, "The gravitational field of phobos," *Geophysical Research Letters*, vol. 16, no. 8, pp. 859–862, 1989.

[2] J. Doyle, A. Packard, and K. Zhou, "Review of lfts, lmis, and mu." Dept. of Electr. Eng., Caltech, Pasadena, CA, USA, 1991.

[3] T. Duxbury and J. Callahan, "Pole and prime meridian expressions for phobos and deimos." *Astronomical Journal*, vol. 86, no. 11, pp. 1722 – 1727, 1981.

[4] A. Falcoz, C. Pittet, S. Bennani, A. Guignard, C. Bayart, and B. Frapard, "Systematic design methods of robust and structured controllers for satellites." *CEAS Space Journal*, vol. 7, no. 3, pp. 319 – 334, 2015.

[5] R. Farquhar, "The control and use of libration-point satellites." p. 214, 1968.

[6] K. Howell, "Three-dimensional, periodic, 'halo' orbits." *Celestial Mechanics*, vol. 32, no. 1, pp. 53 – 71, 1984.

[7] Z. Junjun, N. Dauphas, A. Davis, I. Leya, and A. Fedkin, "The proto-earth as a significant source of lunar material." *Nature Geoscience*, vol. 5, no. 4, pp. 251 – 255, 2012.

[8] E. Kolemen, N. Kasdin, and P. Gurfil, "Multiple poincare sections method for finding the quasiperiodic orbits of the restricted three body problem." *Celestial Mechanics and Dynamical Astronomy*, vol. 112, no. 1, pp. 47 – 74, 2012.

[9] A. Marcos and S. Bennani, "Lpv modeling, analysis and design in space systems: Rationale, objectives and limitations." in *Papers - American Institute of Aeronautics and Astronautics*, ser. Guidance, navigation and control, vol. 1, 2009, pp. 286 – 308.

[10] J. M. Mondelo González and G. Gómez, "The dynamics around the collinear equilibrium points of the rtbp." 2001.

[11] P. Simplicio, A. Marcos, E. Joffre, M. Zamaro, and N. Silva, "Parameterised laws for robust guidance and control of planetary landers," in *4th CEAS Specialist Conference on Guidance, Navigation and Control (EuroGNC 2017), Warsaw, Poland, April 2017*.

[12] V. Szebehely, *Theory of orbit : The restricted problem of three Bodies.* Academic Press, 2012.

[13] M. Zamaro, "Natural and artificial orbits around the martian moon phobos," Ph.D. dissertation, University of Strathclyde, 10 2015.

[14] M. Zamaro and J. D. Biggs, "Dynamical systems techniques for designing libration point orbits in proximity of highly-inhomogeneous planetary satellites: Application to the mars-phobos elliptic three-body problem with additional gravity harmonics." *AIP Conference Proceedings*, vol. 1637, no. 1, pp. 1228 – 1240, 2014.